END
DATE
FILMED
9-81
DTIC

LEVEL II

FLOW RESEARCH COMPANY

A DIVISION OF FLOW INDUSTRIES, INC.

AD A103179

DTIC
ELECTE
AUG 24 1981
D
D

HEADQUARTERS
21414 - 68th Avenue South
Kent, Washington 98031 (206) 872-8500
Seattle Ex. 622-1500 TWX 910-447-2762

81 7 17 084

LEVEL II

(9)

(14) FL N RK-163

Flow Research Report No. 165

Beaufort Sea Ice Mechanical Energy Budget 1975 - 76

By

D. R. Thomas

R. S. Pritchard

August 1980

Flow Research Company
A Division of Flow Industries, Inc.
21414 - 68th Avenue South
Kent, Washington 98031
(206) 872 - 8500

DTIC
ELECTE
AUG 24 1981
S   D
D

390409

Acknowledgment

-i-

Table of Contents

List of Figures

List of Figures (Cont.)

1. Introduction

The mechanical energy budget of the Arctic sea ice cover has only recently been studied. Knowledge of this energy budget helps us understand better the processes by which energy is transferred between the atmosphere and the ocean. The mechanical energy budget provides simple scalar variables that are useful for quantifying sea ice dynamic events. For example, the history of energy transferred to the ice by winds is a useful indicator of the strength of storms. Although energy transfers cannot be observed directly as can be velocity or other kinematic variables, the energy variables are useful when verifying and tuning ice dynamics models.

Long-term observations of sea ice motions in the Beaufort Sea show the general pattern to be a clockwise gyre centered at about $76^{\circ}N$, $145^{\circ}W$ with a period of up to 10 years. Superimposed upon this trend are a great deal of smaller perturbations. Thorndike and Colony (1980) have looked at the spectral density of velocity measurements at stations located on the ice. Spectral distributions of velocity are strongly weighted toward lower frequencies. Energy falls off rapidly at roughly a 5-day period. Coon and Pritchard (1979) developed the equation of balance of mechanical energy by forming the inner product of the ice velocity and the ice momentum-balance equation. Pritchard et al. (1979) used the energy balance concept to describe spatial and temporal variations in the energy budget during a 17-day simulation of the Beaufort Sea ice motion using the AIDJEX model. Comparisons of model results and observed atmospheric and oceanic energies were made.

Noise under the ice in the Arctic Ocean has also been observed and recorded. The background noise is thought to be due to wind-blown snow, the breaking of ice by thermal stresses, and the breaking, sliding, and crushing of ice during ridge building. Ridging seems to dominate other noise sources. Seasonal differences have been observed in noise levels (Greene and Buck, 1977). Correlations between noise level and winds are significant (Greene and Buck, 1978) but explain only between one-third to one-half of the variation. Correlations between noise and wind speed squared are somewhat better (C. R. Greene, personal communication).

In this report, we present and describe the mechanical energy budget of the Beaufort Sea for one year (during the AIDJEX main experiment, 1975-76). We also present some preliminary evidence to verify the conjecture that the energy dissipated in the deformation of the ice cover is related to the background noise level.

2. Mechanical Energy Budget

Coon and Pritchard (1979) formulated a mechanical energy balance for sea ice by forming the inner product of the momentum-balance equation and the ice velocity. The local form of this mechanical energy balance can be written as a balance between the time rate of change of kinetic energy (areal) density $\dot{k}$ and the rate of energy transfer (areal) from the atmosphere p_a to the ocean p_w and the ice p_i :

$$\dot{k} = p_a - p_w - p_i \ . \tag{1}$$

All energy transfer rates were computed as daily, averaged energy transfers per unit area. For brevity we shall use the term "energy transfer rate." The kinetic energy density of the ice cover is

$$k = 1/2 \ m\underset{\sim}{v}^t\underset{\sim}{v} \ , \tag{2}$$

where m is areal mass density, $\underset{\sim}{v}$ is the ice velocity, and $\underset{\sim}{v}^t$ is the transpose of $\underset{\sim}{v}$. The rate of energy transfer from the atmosphere

$$p_a = \underset{\sim}{v}^t\underset{\sim a}{\tau} \tag{3}$$

is the rate at which energy is transferred from the atmosphere to the top surface of the ice due to the air drag $\underset{\sim a}{\tau}$. The rate of energy transfer to the ocean is similarly

$$p_w = -\underset{\sim}{v}^t \left[\underset{\sim w}{\tau} - mg\nabla H \right] \ , \tag{4}$$

where $\underset{\sim w}{\tau}$ is the water drag, ∇H represents sea surface tilt, and g is the gravitational acceleration. Negative values of p_w imply that the ocean currents are driving the ice. The oceanic energy transfer rate p_w has been decomposed by Pritchard et al. (1979) into the rate of energy transfer to the ocean due to water drag $\underset{\sim w}{\tau}$ and the rate of change of gravitational potential energy due to sea surface tilt

$$p_w = p_o + p_g \ , \tag{5}$$

where $$P_o = -\underset{\sim}{v}^t \underset{\sim}{\tau}_w \tag{6}$$

and $$P_g = \underset{\sim}{v}^t mg\nabla H . \tag{7}$$

The remaining term in the mechanical energy balance equation (Equation (1)) P_i represents the influence of internal ice stress on the transfer of energy from the atmosphere to the ocean

$$P_i = -\underset{\sim}{v}^t (\nabla \cdot \underset{\sim}{\sigma}) , \tag{8}$$

which can in turn be separated into two parts

$$P_i = -P_f + P_d , \tag{9}$$

where $$P_f = \nabla \cdot (\underset{\sim}{v}^t \underset{\sim}{\sigma}) \tag{10}$$

is the divergence of the stress flux (i.e., the rate of energy transfer horizontally through the ice) and

$$P_d = \text{tr } \underset{\sim\sim}{\sigma D} \tag{11}$$

is the trace of the product of stress and stretching or the rate at which energy is dissipated by the internal stress through deformations. For the elastic-plastic model used in this work (see Appendix A), P_d may be either stored as recoverable or elastic strain energy $U_e = \text{tr } \underset{\sim\sim}{\sigma e}$ or dissipated by plastic deformation $P_\ell = \text{tr } \underset{\sim\sim p}{\sigma D}$. The quantities are related by

$$P_d = \dot{U}_e + P_\ell . \tag{A.6 bis}$$

Our approach in this work is to approximate P_d by P_ℓ , the difference $\dot{U}_e$ being small as shown in Appendix A. The term U_e is considered an error term which can be arbitrarily small.

The term P_d represents the rate of energy storage or dissipation in the ice cover. Dissipation occurs when ice blocks slide along one

another (friction), when ice floes break, and when ice blocks are piled into ridges (increase in potential energy). Observers have noted that ridge building is accompanied by a great deal of noise and is the largest source of noise in the central Arctic pack (B. M. Buck, personal communication). Thus, a majority of the noise energy in the Arctic is a by-product of the ice deformation.

Three of the terms in the energy balance given in Equation (1) may be computed directly from observed data. These are $\dot{k}$, p_a, and p_w (or p_o and p_g). Changes in kinetic energy involve only observed ice thickness and ice velocity. Energy input from the atmosphere depends upon ice velocity, geostrophic or surface winds, and a drag law. The quadratic law in terms of geostrophic winds $\underset{\sim}{U}$ is

$$\underset{\sim}{\tau}_a = \rho_a C_a |\underset{\sim}{U}| \underset{\sim}{A} \underset{\sim}{U}$$

$$\underset{\sim}{A} = \begin{pmatrix} \cos \alpha & -\sin \alpha \\ \sin \alpha & \cos \alpha \end{pmatrix}.$$

(12)

where $\rho_a C_a = 0.035 \text{ kg/m}^3$ and $\alpha = 24°$ are typical values (Leavitt et al., 1978; M. Albright, personal communication). The energy transfer rate to the ocean depends upon ice velocity and mass, geostrophic currents, and an oceanic drag law. A quadratic form of the drag law is again used

$$\underset{\sim}{\tau}_w = \rho_w C_w |\underset{\sim}{v} - \underset{\sim}{v}_g| \underset{\sim}{B}(\underset{\sim}{v} - \underset{\sim}{v}_g)$$

$$\underset{\sim}{B} = \begin{pmatrix} \cos (\pi + \beta) & -\sin (\pi + \beta) \\ \sin (\pi + \beta) & \cos (\pi + \beta) \end{pmatrix},$$

(13)

where $\rho_w C_w = 5.5 \text{ kg/m}^3$ and $\beta = 23°$. The parameters C_w and β have been experimentally determined, and the form of the drag law has been tested (McPhee, 1980). The geostrophic ocean current $\underset{\sim}{v}_g$ is approximated by the long-term mean flow according to Newton's (1973) dynamic topography.

Since all except one of the terms in Equation (1) may be calculated from observed data, the rate at which energy is transferred into the

ice p_i can be computed as a residual of the other terms. However, p_d and p_f , which are combined in p_i , cannot be computed directly from observed data since the ice stress cannot be measured directly. A material model of the ice is required in order to determine the stress and compute the energy dissipation rate p_d .

In order to quantify the wind energy available, we have computed the maximum possible transfer rate of energy from the atmosphere to the ice and the ocean. This maximum transfer occurs when ice stresses are zero and the ice moves freely with the wind. Energy from the atmosphere is transferred to the ice at the rate p_{afd} , and then through the ice into the ocean at the rate p_{wfd} , or it goes into changing the kinetic energy $\dot{K}_{fd}$:

$$\dot{K}_{fd} = p_{afd} - p_{wfd} \; . \tag{14}$$

3. Data

Computation of the terms in the mechanical energy budget requires
knowledge of the ice velocity, surface winds, and ocean currents, as
well as the internal ice stress. The ice stress cannot be measured
directly, but stresses can be modeled using a complete ice dynamics
model driven by winds and currents (Coon et al., 1974; Pritchard, 1980;
Hibler, 1980) or by using observed strain history in the constitutive
laws (Rothrock et al., 1980). During the AIDJEX main experiment from
1975-76 a vast quantity of data about the ice in the Beaufort Sea was
collected. Satellite-tracked buoys were used to determine ice motions.
Buoy data processing and ice motions have been described by Thorndike
and Cheung (1977). Part of the processing involved smoothing the position
data to reduce the satellite positioning error. As a result, much of
the higher frequency motion (in less than a 24-hour period) is attenuated.
Thorndike and Colony (1980) have shown that most of the ice deformation
occurs at low frequencies. Since we are only concerned with time scales
of a day or greater in this study, we performed additional filtering of
the ice motion data to remove all frequencies greater than one day.

In Figure 1 we show the amount of buoy position data used in this
study, and in Figure 2 we show the approximate location of each buoy on
January 30, 1976. In addition to position, each of these buoys measured
barometric pressure. From the derived pressure maps, geostrophic wind
fields were calculated for the Beaufort Sea (Albright, 1980). The
surface traction exerted on the upper side of the ice is related to the
geostrophic flow (Brown, 1976) by Equation (12). To be consistent with
ice motion data, atmospheric surface traction fields $\underset{\sim a}{\tau}$ were computed
every 6 hours and then filtered to get daily average values.

Seasonal values of the mean ice thickness $\bar{h}$ are computed by
Thorndike et al. (1975). A comparison of the April value of $\bar{h}$ as
measured by an under-ice sonar profile (Wadhams and Horne, 1978) agrees
with the tabulated value within 5 percent.

Noise data were also collected at eight of the buoy stations (those
marked with solid dots in Figure 2). Sound pressure levels are available
(Burke and Buck, 1975). These are values for 1/3 octave bands centered
upon 3.2, 10, 32.0, and 1000 Hz (at one station 100 Hz instead of 3.2 Hz
was sensed). Pressure histories sensed by hydrophones were filtered
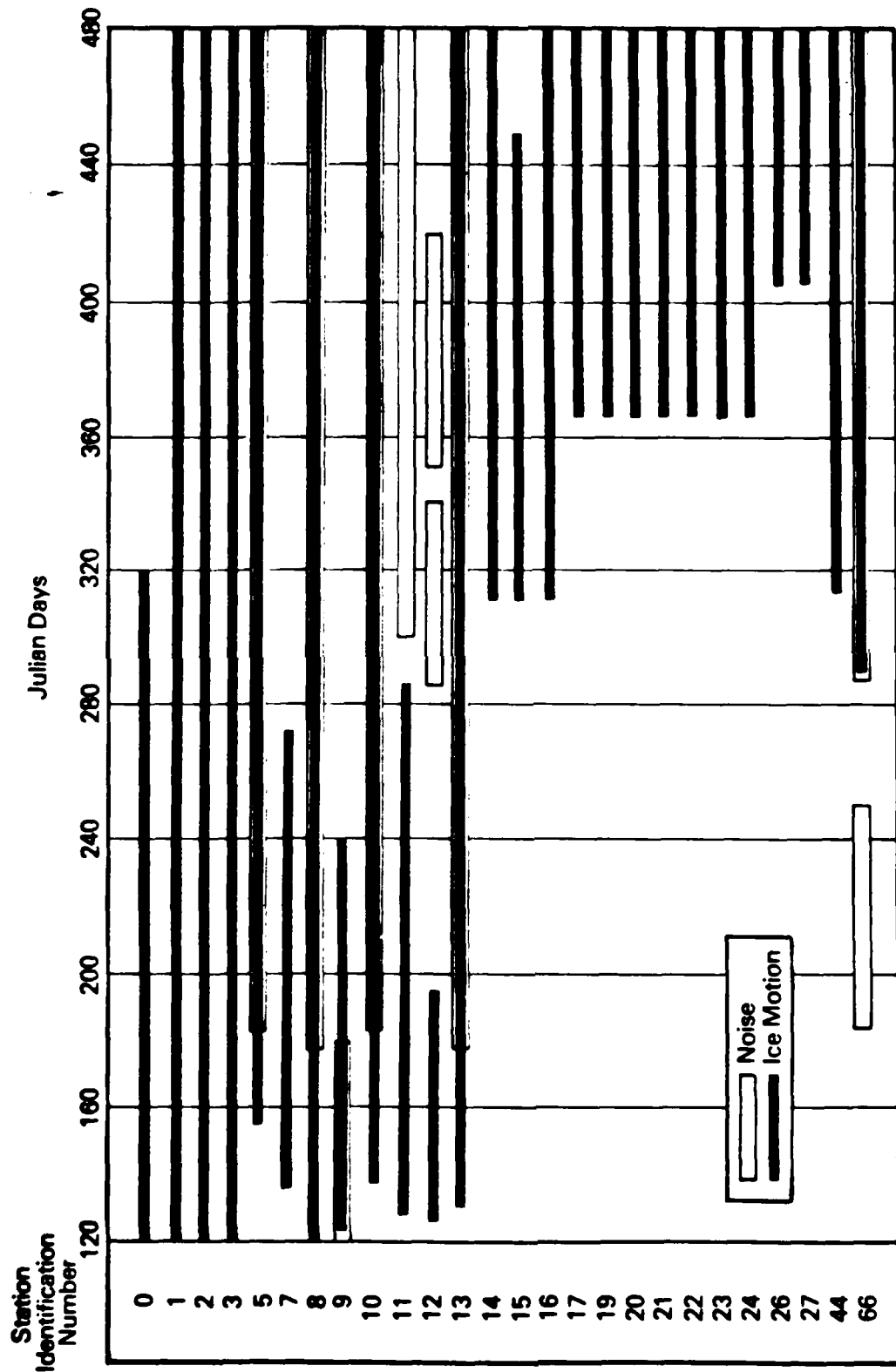
Figure 1. Bar Graph Showing When Ice Velocity Data Are Available at Each Station (Heavy Line). Hydrophone Data Was Obtained at Some Stations for Periods Indicated by Double Thin Lines. Day 121 Is May 1, 1975.
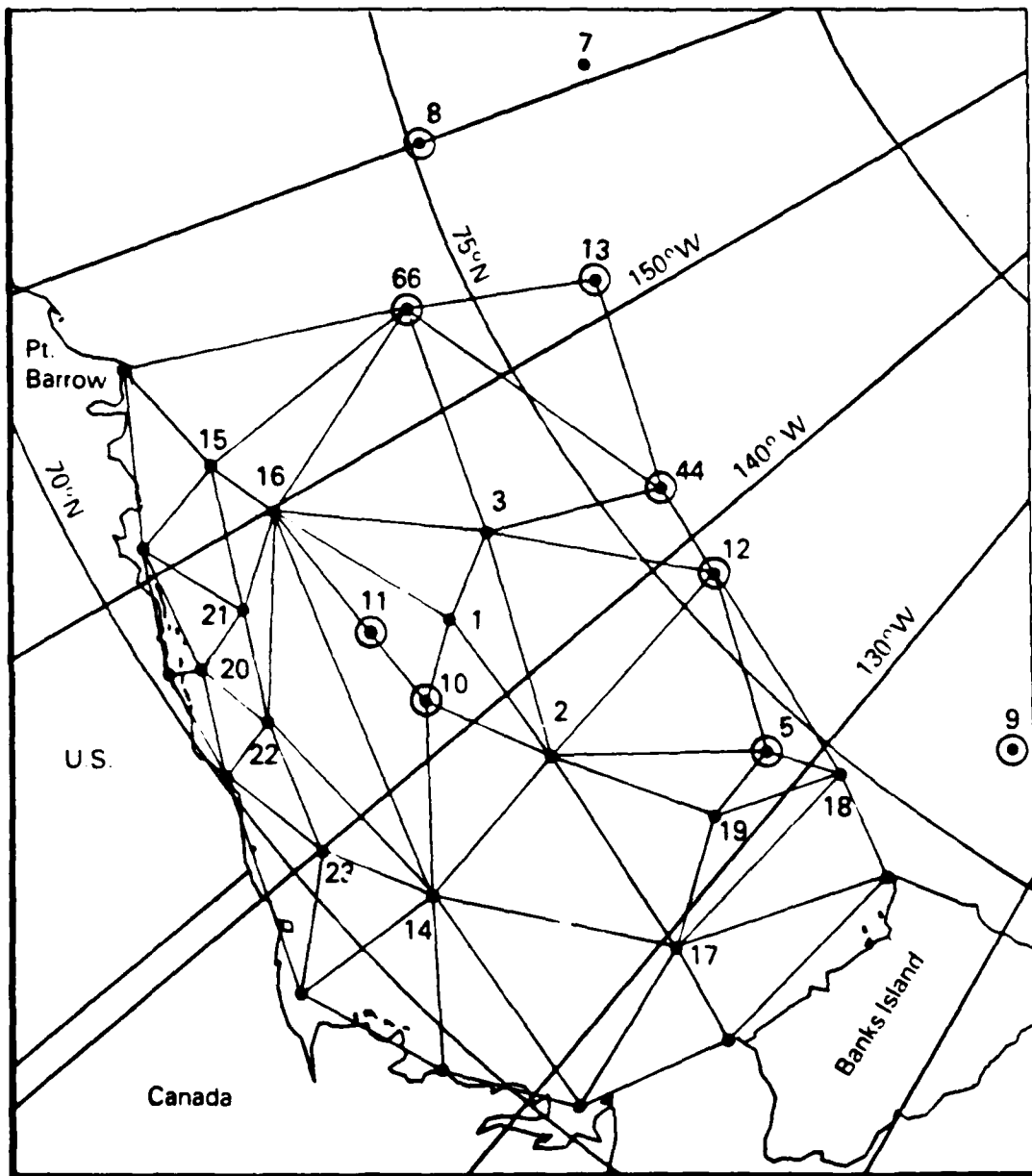
Figure 2. Location of Operative Data Buoys, Midwinter 1975-76. Buoys Marked With Solid Circles Collected Acoustic Data As Well As Position and Atmospheric Pressure.

into 1/3 octave bands, averaged over 45 second intervals, and then
sampled each 3 hours. The 3.2 Hz signal has been noted to be contam-
inated by self noise from the hydrophone (Greene and Buck, 1977) and has
therefore not been included in this study. It is traditional that
acoustic data are presented as logarithms of the pressure (or intensity)
normalized by a reference value. However, to make a comparison between
observed noise levels and the energy budget components, we present all
data in a linear scale rather than a logarithmic scale. We also focus
on the intensity of the acoustic signal, rather than the pressure,
because it is the desired measure of energy in the signal.

4. Observed Energy Transfer from Atmosphere to Ice to Ocean

At each station a time history of the daily average rate of energy density transferred from the atmosphere to the ice p_a and between the ice and the ocean p_w is computed. Also, the energy transfer rate from the atmosphere to the ice assuming no internal ice stress p_{afd} is computed, in which case all the atmospheric energy is transferred through the ice and into the ocean. This term is useful as a measure of the maximum energy available to move and deform the ice. The changes in kinetic energy from day to day $\dot{k}$ is also computed at each station. This term is less than 1 mW/m^2 and is therefore insignificant when compared to other terms in the energy balance. Evaluating $\dot{k}$ and showing it to be negligible proves that the energy budget may be assumed to be quasistatic on 1 day resolution. The change in potential energy due to sea surface tilt is also negligible. The variable p_g is usually less than 1 mW/m^2 and always less than about 5 mW/m^2. Therefore, the rate of energy transfer to the ocean p_w is nearly equal to the energy transferred via water drag p_o.

Figure 3 shows that time histories of energy transfer rates are characterized by events of 3 to 7 days duration followed by quiet periods of approximately the same length. These events are atmospheric storms passing over the Beaufort Sea. The p_{afd} term is a useful measure of the intensity of storms since it amplifies the winds (p_{afd} is roughly proportional to U^3, the wind speed cubed). Note that computation of p_{afd} requires only the observed winds and p_a uses the observed winds and the observed ice motion, whereas p_w is calculated from only the observed ice motion. Thus two independent data sets are used. Even though the data sets are independent, there are strong similarities between the traces of p_a, p_w, and p_{afd}. Peaks occur simultaneously and shapes are similar in period and phase. This gives confidence that winds and motions are accurate.

The difference in the history of p_a and p_w is p_i, the rate at which energy is transferred horizontally through the ice or dissipated by ice deformation. The effect of ice stress is seen to increase during winter when ice strength is high. This is seen in both p_i and in $p_{afd} - p_w$, the effect of ice stress on the rate of energy transfer into the ocean.
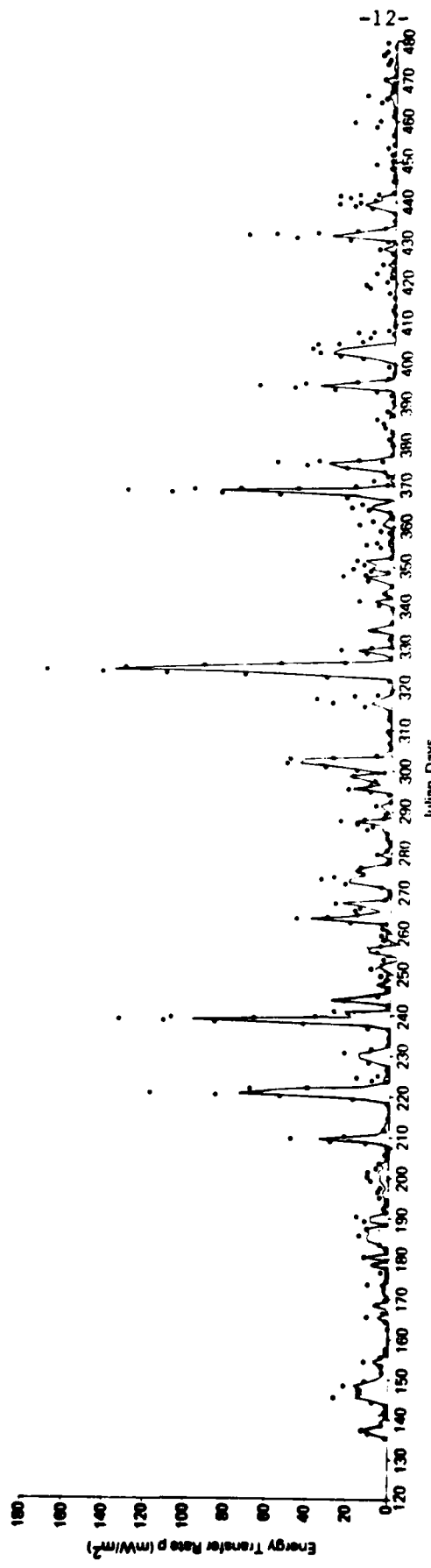
Figure 3. Time History of P_B (— — —), P_W (———), and P_{sfd} (·····) at Station 10.

Energy Transfer Rate ρ (mW/m²)

Julian Days
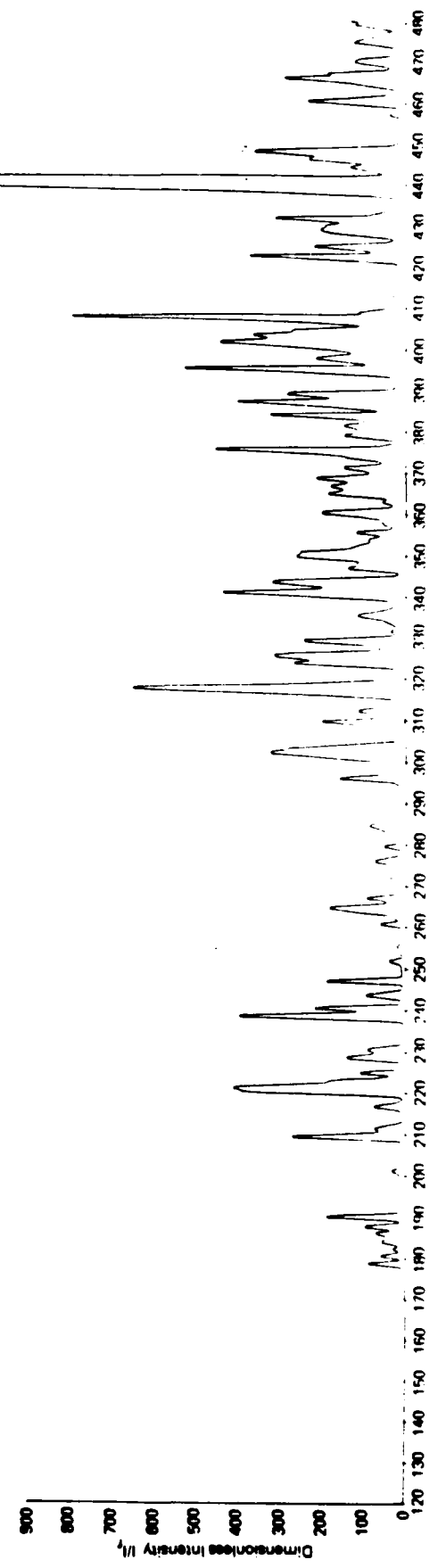
Figure 7 Time History of 10 Hz, 1/3 Octave Spectral Band of Sound Intensity at Station 10

Dimensionless Intensity I/I_r

Julian Days

For reasons of space, we do not present time histories for all stations but note that all look similiar. However, two kinds of spatial variability were evident in the plots. Peaks at widely separated locations may differ in magnitude partly due to spatial scales which are about the same size as the atmospheric low pressure system. Also, a frequent temporal shift of a day or two in the peaks at different locations can be caused by a storm moving across the study area.

The data $(P_a, P_w,$ and $P_{afd})$ from each station with records longer than 60 days were put through a 31-day boxcar filter. The resultant month-long averages for all stations are plotted together in Figure 4 along with the mean of all stations. This figure displays both the spatial variability across the Beaufort Sea and the long-term seasonal trends of the energy transfer rates. Much of the the time, the total spatial variations in P_a, P_w, and P_{afd} are within 2 to 3 mW/m^2 or about 20 to 40 percent of the mean value. At other times when variability is large, only two or three stations are causing the increase in spatial variability. In any case, the spatial average is descriptive of time histories at each site. A definite seasonal variation can be seen. There is a maximum in late summer, that remains fairly high. Another peak occurs in late November and early December, then decreases through spring and early summer. Generally the spatial variation is less than the seasonal trends.

As a further illustration of seasonal differences in P_a, P_w, and P_{afd}, we present in Figure 5 histograms of daily average energy transfer rates for 3-month periods. Histograms were not done for spatial variation because of lack of data points. Bin sizes in all these histograms are 5 mW/m^2. The first bin contains the background signal, those days with little or no wind and ice motion. The last bin (shaded) contains all values greater than 50 mW/m^2. The three sets of histograms are very similiar. The summer months (July, August, September) show the most activity with fall and winter (October through March) similar to each other and having intermediate activity. Spring (April, May, June) has the least activity.
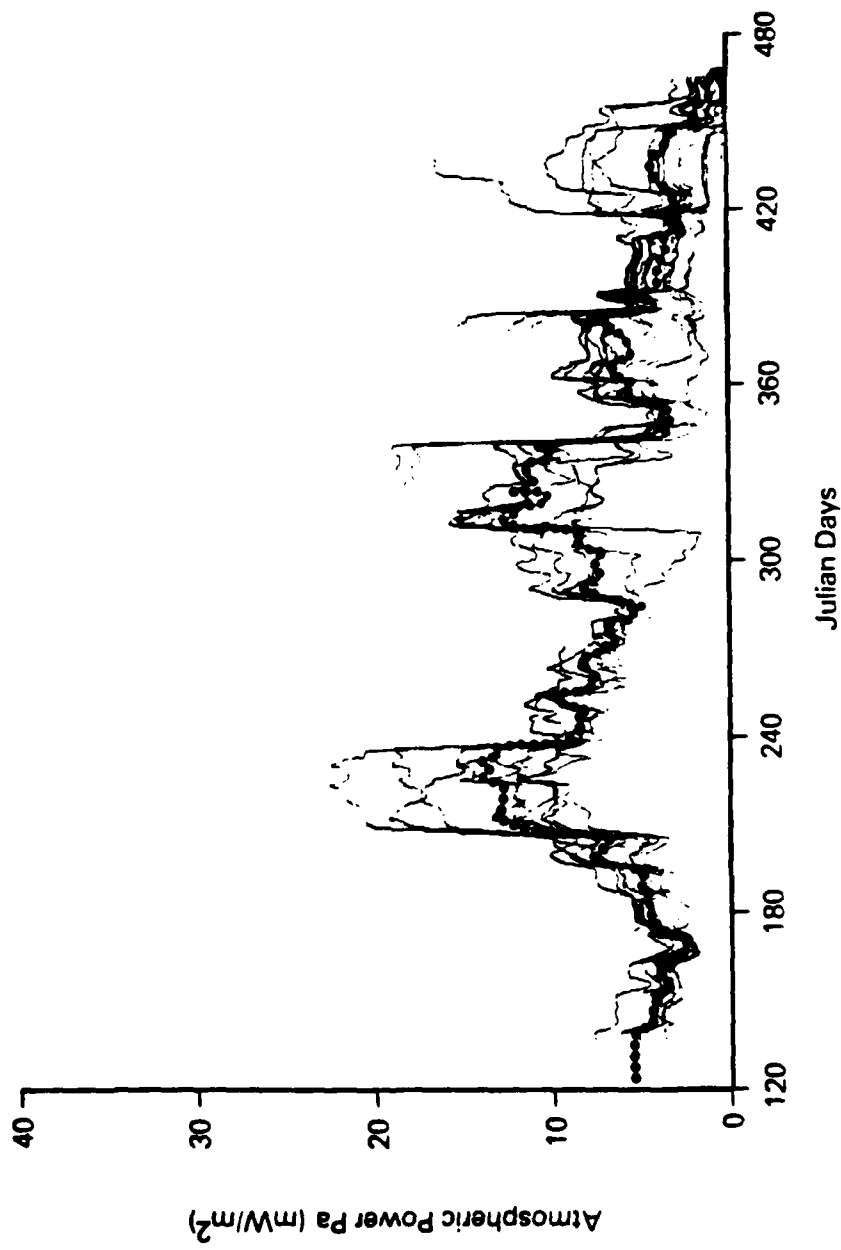
Figure 4a. Time History of 31-Day Moving Average of Power Input from the Atmosphere. Individual Curves Represent Different Locations and the Heavy Dotted Curve is the Mean of all Stations.
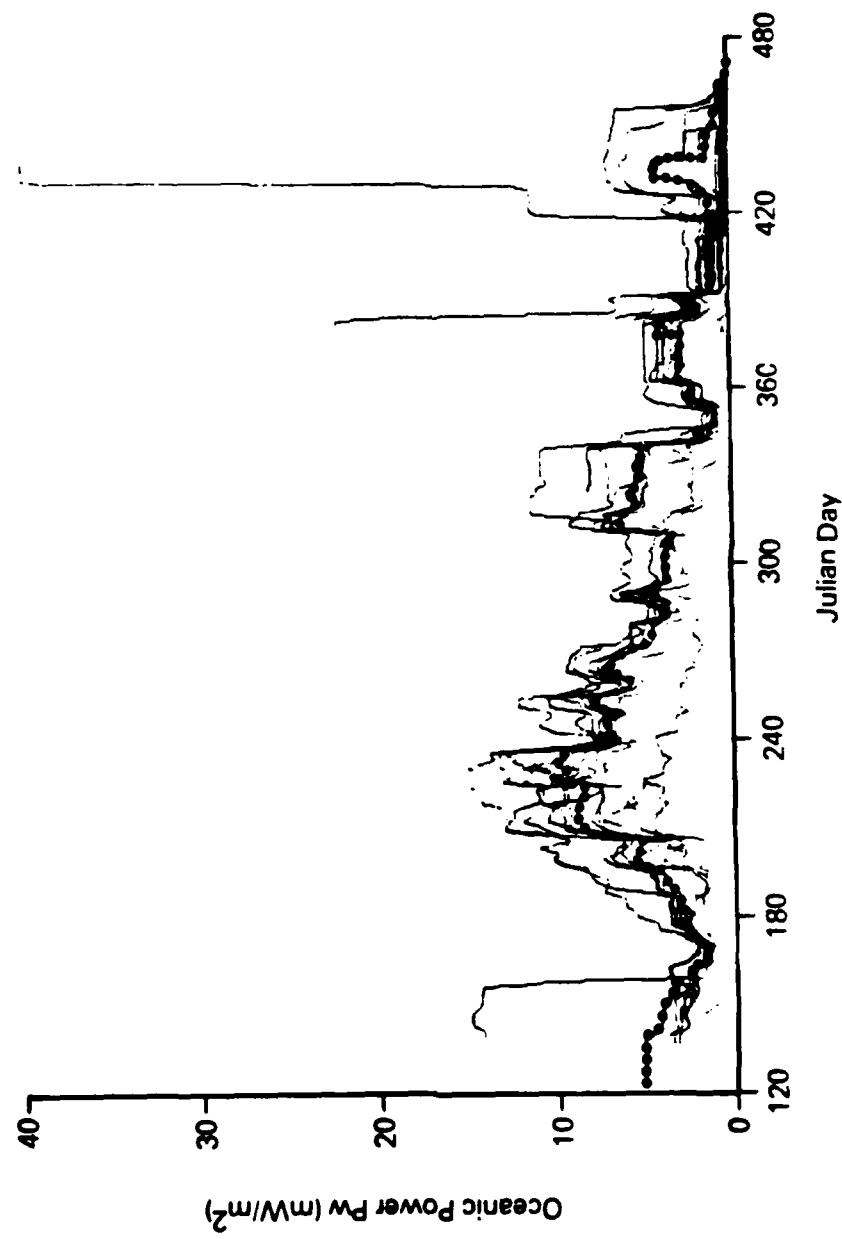
Figure 4b. Time History of 31-Day Moving Average of Power Input to the Ocean. Individual Curves Represent Different Locations and the Heavy Dotted Curve is the Mean of all Stations.
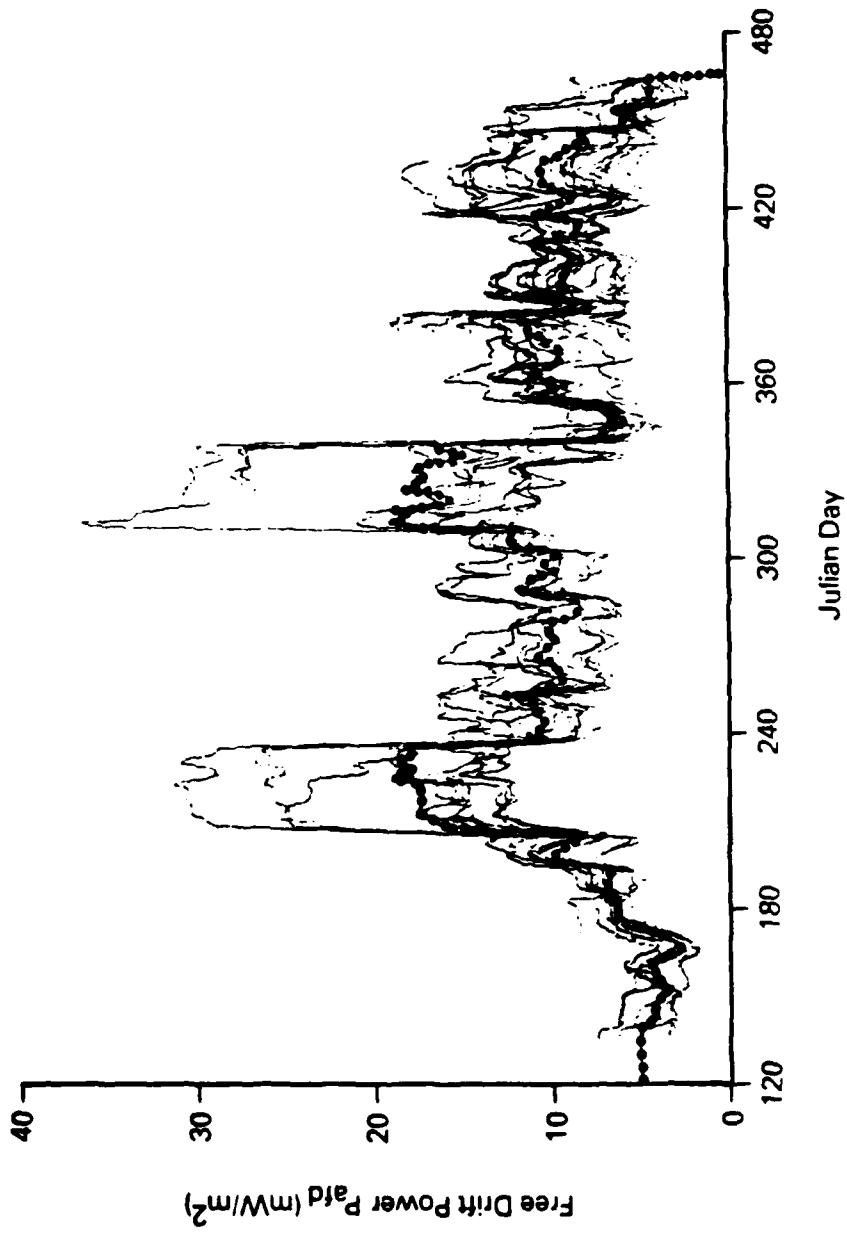
Figure 4c. Time History of 31-Day Moving Average of Free Drift Power Available. Individual Curves Represent Different Locations and the Heavy Dotted Curve is the Mean of all Stations.
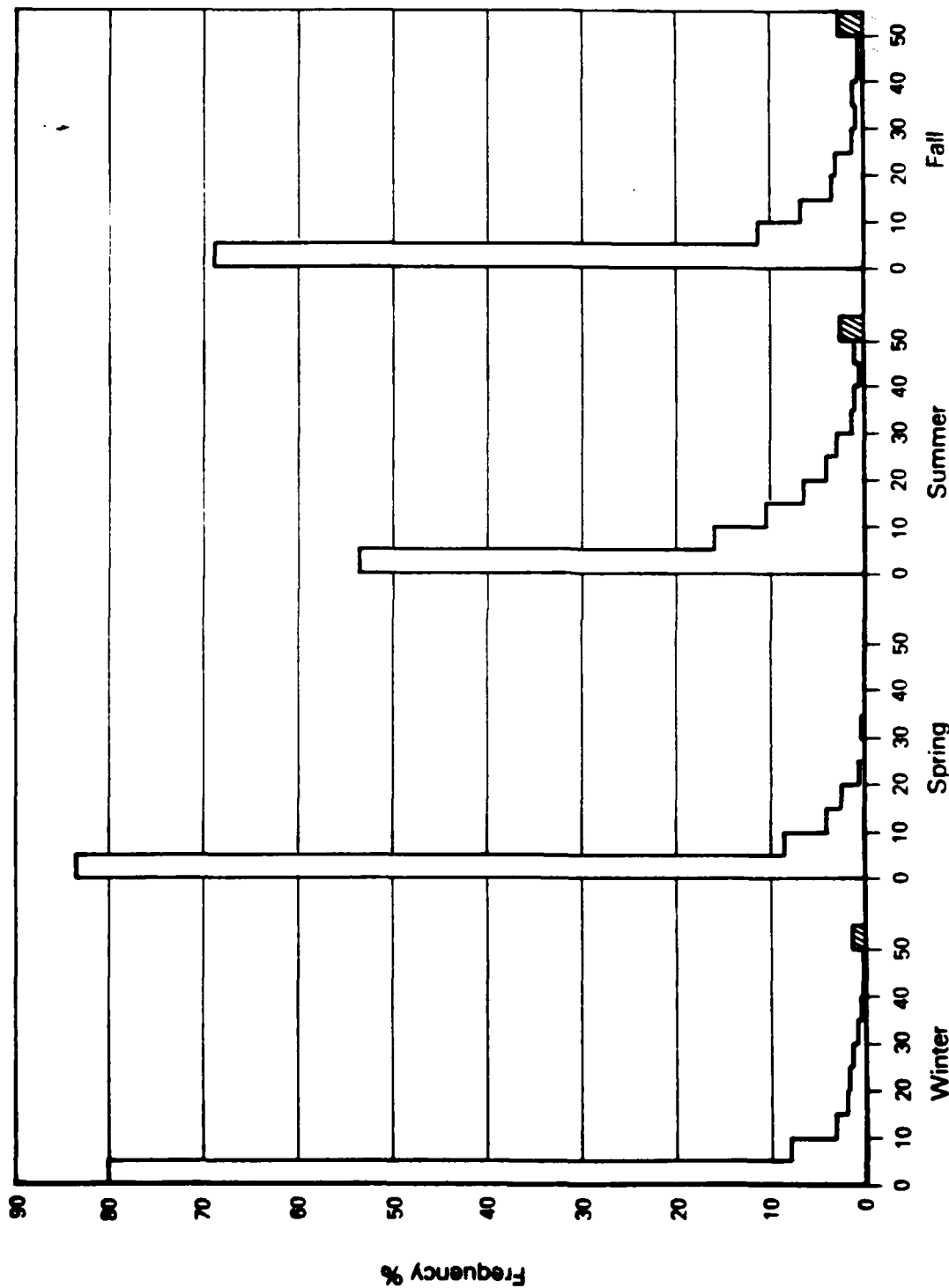
Figure 5a. Daily Average Values of Power Input from the Atmosphere p_a (mW/m^2). Vertical Scale is Percentage of Observations During the Season at all Locations.
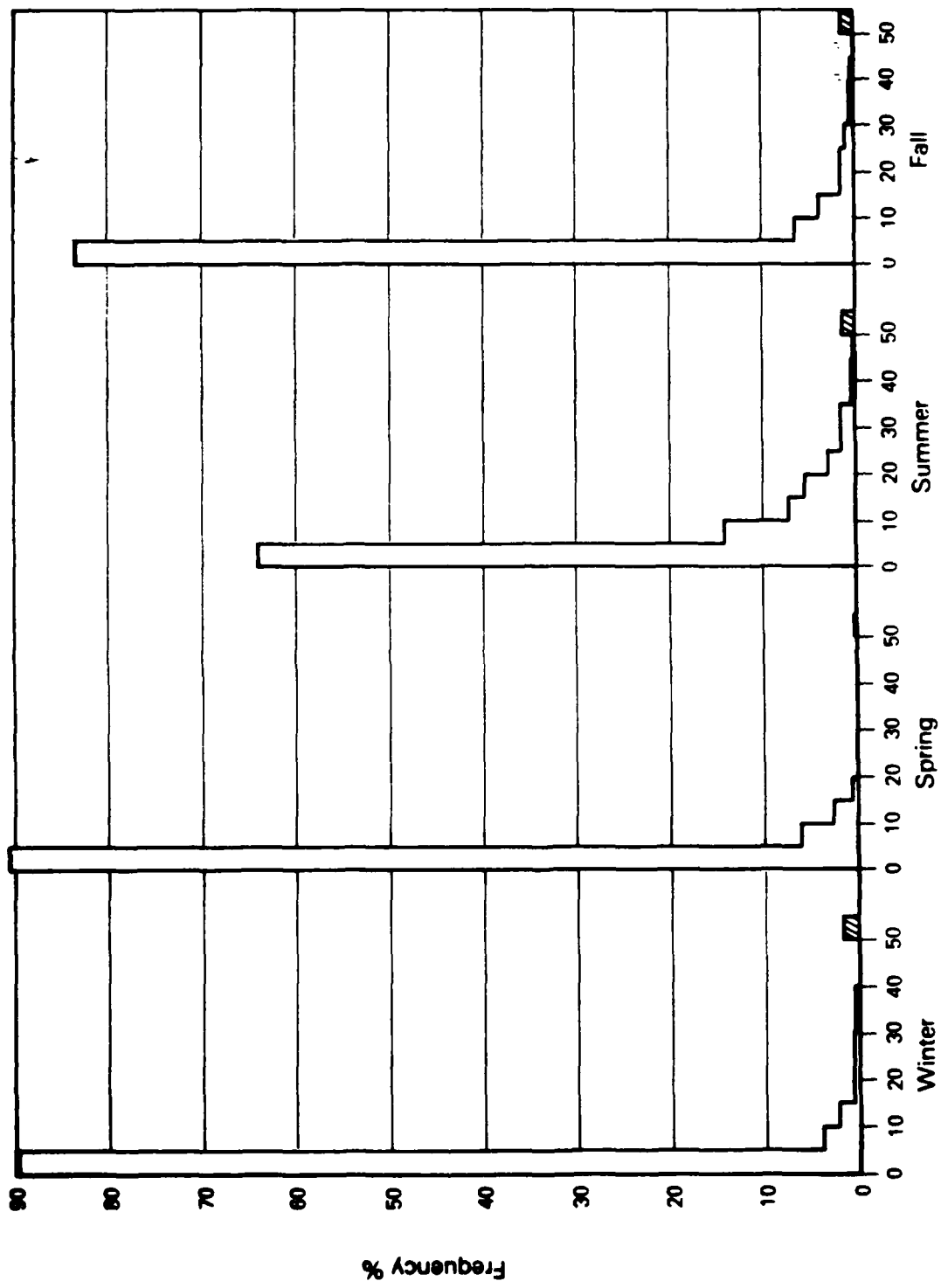
Figure 5b.   Daily Average Values of Power Input to the Ocean p_w (mW/m^2). Vertical Scale is Percentage of Observations During the Season at all Locations.
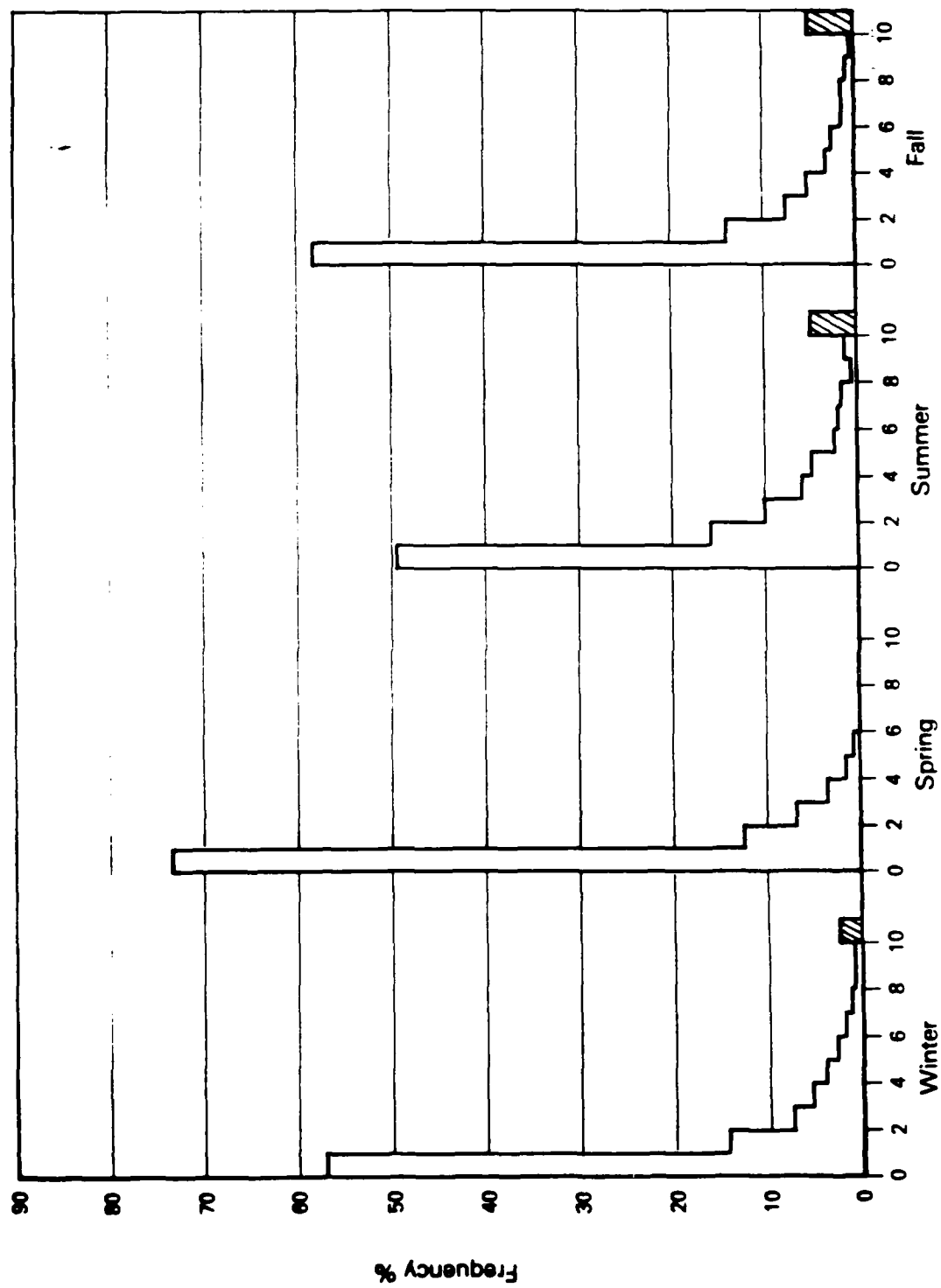
Figure 5c.   Daily Average Values of Free Drift Power Available p_{afd} (mW/m^2). Vertical Scale is Percentage of Observations During the Season at all Locations.

5. Dissipation of Energy by Sea Ice

From Equation (1) we see that we can easily compute $p_i = p_a - p_w$, the net rate of energy transfer into the ice cover. But the energy transferred into the ice can either be transferred horizontally into some other region by the ice stress divergence or dissipated by deforma- tion of the ice cover. As a result, more information about the stress field is needed to separate p_i into these two components. Thus, either the net horizontal energy transfer rate into or out of a region p_f (the divergence of stress flux) or the rate of energy dissipated by ice deformation inside the region p_d must be computed directly in order to describe completely the mechanical energy balance for a region. To compute either of these terms, the internal stresses in the ice must be known. Since these large-scale stresses cannot be measured directly, some form of ice model is needed to estimate the stress from the deformation and divergence properties of the ice.

The deformation history may be used directly as input to the constitutive law (see Appendix A) to calculate the stress history. From this pair of variables the rate of energy dissipation by plastic deformation p_ℓ is calculated directly as an approximation to p_d . In the full AIDJEX ice model, described in Appendix A, the strength parameter p* is computed from the ice thickness distribution. During most of the time period of this study we have inadequate data on the actual ice thickness distribution. Fortunately, during parts of the year this is not a critical factor. McPhee (1980) has shown that during the summer of 1975, the ice was usually in a state of free drift, i.e., the stresses were negligible. During the depths of winter, Pritchard (1980) has shown that the ice strength is very high. Some spatial and temporal variation will be lost by assuming the strength to be constant and every- where high. During the fall, when ice is growing on the large amounts of open water, or in the spring, when ice is melting and new areas of open water are being produced, the variations in ice strength are likely to be much greater than in the winter or summer. We therefore decided to consider only the summer and winter periods when looking at the p_d term.

During the winter then, the simplified version of the AIDJEX model is used in which strain rates are computed from observed velocities at three locations forming a triangle. The strain rates were used to compute stresses, assuming a constant ice strength of $p^* = 10^5$ N/m . The energy dissipated by the ice in plastic deformation ($p_\ell = \text{tr } \underset{\sim}{\sigma} \underset{\sim}{D}_p$) is computed since both $\underset{\sim}{D}_p$ is available from data and $\underset{\sim}{\sigma}$ can be calculated from the model.

Thorndike and Colony (1977) have demonstrated that estimates of the deformation gradient from the velocity of a few floes are subject to large error. They argue that discontinuities in motion between floes are large enough that the smooth velocity field (on length scales of 100 km) accounts for only about two-thirds of the variations. By fitting locally linear surfaces to the velocity field, and measuring errors in this fit, standard deviations of the linear and nonlinear contributions to the velocity field are calculated, as shown in Table 1. Daily averages are considered in all cases.

Table 1. Estimated Variability of Daily Velocity Over
100 km. Tabulated Values are Estimated RMS
Values with 90 Percent Confidence.

Time	Linear Component km/day	Nonlinear Component
May 1 - Jun 29, 1975	1.0	0.4
Jul 30 - Sep 17, 1975	1.6	1.0

Interpreting the results presented in Table 1, we must conclude that deformations calculated by fitting a plane through the velocity values at the three vertices of a triangle of 100-km size may be in error by as much as 0.8 percent per day in May and June 1975 and by as much as 2.0 percent per day during August and September 1975. To estimate the history of p_d , Equation (11), we use the deformation $\underset{\sim}{D}$ to calculate the stress state $\underset{\sim}{\sigma}$. Uncertainties in deformations due to the nonlinear variations introduce uncertainties into the stress state that are large enough to move the stress anywhere on the yield surface (see Appendix A). These uncertainties in both deformation and stress then contribute to uncertainty in p_d . There are no reasons to expect more accurate

-22-

values of deformation $\underset{\sim}{D}$ at other times of the year. Because of
these uncertainties plus the lack of temporal and spatial resolution in
ice strength, we have only computed the average value of P_d . The
triangles and wintertime average values of P_d are plotted on a map of
the Beaufort Sea in Figure 6. The locations of the buoys (triangle
vertices) are correct for about the end of January. Total deformation
of the array of buoys for the 3 winter months was relatively small.

The most noticeable feature of this figure is the spatial varia-
bility in P_d . Average values of P_d nearshore along the north coast
of Alaska are an order of magnitude larger than values in the rest of
the Beaufort Sea. In Figure 4 the spatial variability of the other
energy terms P_a , P_w , and P_{afd} is seen to be only 2 or 3 times
larger. This regional variation in P_d is due to the ability of the
ice to transmit stresses and energy horizontally. Energy input by winds
and currents over the entire Beaufort Sea is then transmitted by the
stress flux divergence and dissipated near the north coast of Alaska.

The spatial distribution of P_d presented here agrees quite well
with the distribution derived from a full AIDJEX model simulation of ice
motion and stresses reported in Pritchard et al. (1980). A 17-day
period (from late January to early February 1976) was modeled and the
results were filtered to obtain average daily values. During the height
of two storms during that period, contour maps of P_d were constructed.
Regional differences in P_d were much greater than we find in the
average winter values, but that is merely the difference between one
individual storm in one case and averaging many storms and quiet periods
in the other. The geographical concentration of P_d is consistent
between the two types of model runs. This fact gives us confidence in
the energy dissipation rate field of Figure 6, even though the deforma-
tions cannot be determined with confidence.

Furthermore, observations of ridge densities in the Beaufort Sea
confirm the distribution of P_d in Figure 6. Laser profiles (Weeks
et al., 1980) off the north coast of Alaska show the heaviest amount of
ridging in the area nearshore with ridge density decreasing towards the
north. Ridge densities just north of the Mackenzie Delta are less than
off the north Alaskan coast (Wadhams, 1975). While the actual magnitudes
of the P_d values in Figure 6 may be incorrect, we are confident of the
spatial variations.
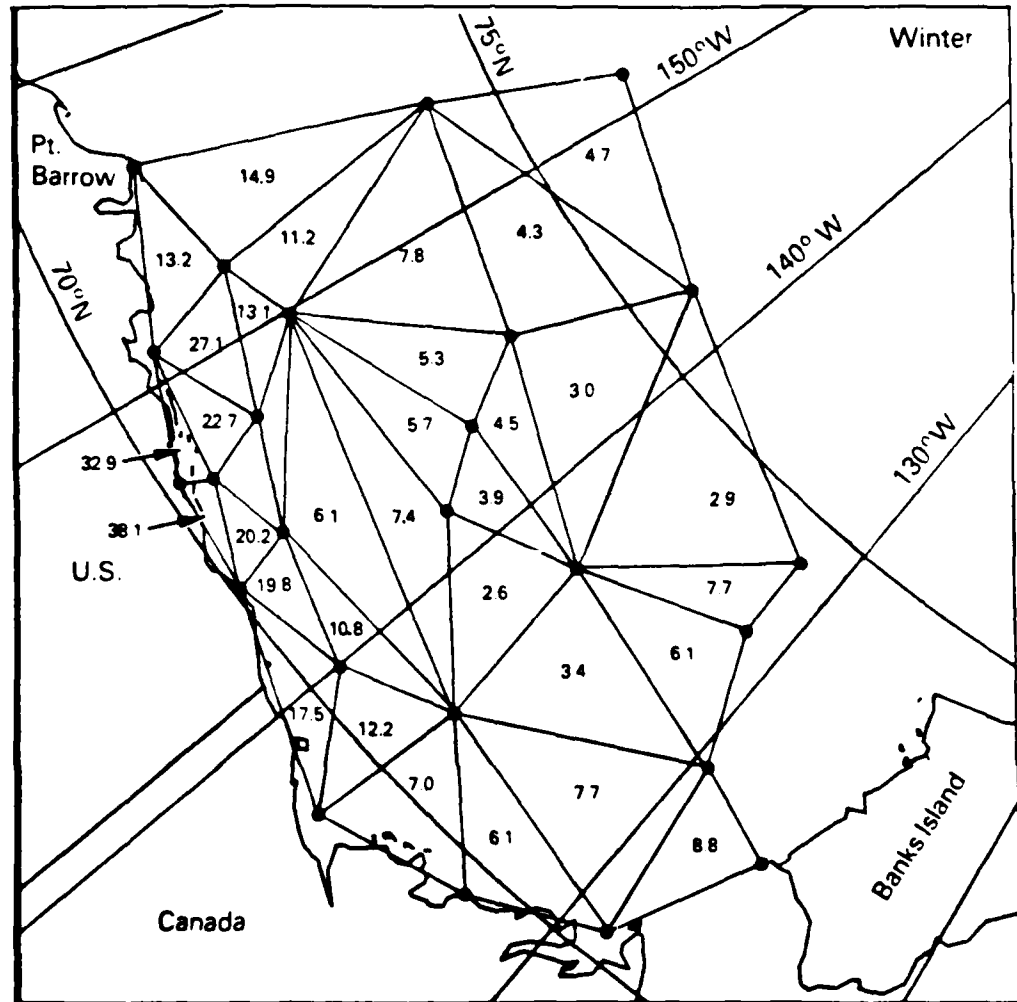
Figure 6. Daily Average Wintertime (Jan-Mar) Values of Rate of Energy Dissipated by Ice (p_d) for 33 Locations in Beaufort Sea, Computed Using Observed Ice Motions and Modeled Stresses.

6. Comparison of Acoustic Data with Energy Dissipated

In Figure 7 we present a time history of the amplitude of the
background signal observed at station 10 (see Figure 2). This result is
the daily average obtained by passing a running 24-hour boxcar filter on
the data set. The noise is the magnitude of the 1/3 octave spectral
band centered at 10 Hz. The reference level is $I_r = P_r^2 = 1 \ \mu Pa^2/Hz$
and a nondimensional amplitude is presented. The fundamental characteristics
of frequency, duration, and relative peak amplitude is similar to the
terms in the energy budget history. This time history is included as an
example of the data set used to obtain the final results.

Acoustic data are normally presented in terms of noise or sound
pressure levels (e.g., Clay and Medwin, 1977; Urick, 1967)

$$SPL = 20 \ \log_{10} \frac{P}{P_r} \ dB \ re P_r \ . \tag{15}$$

This is a useful form for studying sound, but we are more interested in
the energy content of the sound and so we look instead at the sound
intensity level

$$SIL = 10 \ \log_{10} \frac{I}{I_r} \ dB \ re I_r \ . \tag{16}$$

We also have no strong reason to introduce a logarithmic scale. The
linear scale allows us to focus on major storm events in the energy
budget. Therefore, the SPL data obtained from Dr. B. M. Buck (personal
communication) are converted to normalized linear intensity levels
$\frac{I}{I_r} = 10^{SPL/10}$. This quantity is comparable to the unit area energy
transfer rates used in the energy budget and provides the appropriate
measure that can be related to the source energy level of the acoustic
signal.

We should point out that plastic dissipation p_ℓ describes all the
energy dissipated when the elastic-plastic model is used. However,
during ridge formation a substantial component of p_ℓ represents the
increase in gravitational potential energy due to piling ice into sails
and keels. This component is not a strong candidate for explaining
background noise levels. On the other hand, much of p_ℓ can be attributed

to frictional dissipation due to ice blocks sliding over each other
(Rothrock, 1975), and this process is certainly a strong candidate as a
noise source. The bumping, breaking, and tumbling of ice blocks
during ridge building, while not a large energy sink, must also contri-
bute to noise generation. We have not yet attempted to separate these
components of p_ℓ . The strongest reason for making a preliminary
comparison between p_ℓ and noise is that both components satisfy the
same functional form, so each is a fixed percentage of p_ℓ .

Another shortcoming of the present comparison should be mentioned.
We know that sound signals observed at one location are potentially the
result of many sources located at different locations, each propagating
through the ocean (with its respective transmission loss) until reaching
the location of observations. Because of this shortcoming in the
current work, we have not attempted to compare individual signals but
have attempted to show general trends instead.

For comparison with the energy transfer rates p_a , p_w , and
p_{afd} , seasonal histograms were made for the 10 Hz and 1000 Hz intensities
(Figure 8). Note that the distribution of values is similar for both
frequencies. The lowest levels of sound intensity are more frequently
observed during the summer months, while fall and winter have the
predominance of higher intensity signals.

The observed energy transfer rates, on the other hand, had a higher
percentage of large values during the summer. The lowest percentage of
large values occurred in the spring with fall and winter having intermediate
values. Our conjecture is that the energy dissipated by the ice in
noise-generating processes is more closely related to observed noise.
Computed values of wintertime dissipation are large and we conclude that
summertime values of p_d would be an order of magnitude or more smaller
than winter values. Thus, seasonal variations in p_d are more in
agreement with observed acoustic energies than are p_a , p_w , or p_{afd} .

Spatial variation in the sound intensity more closely resembles
the variation in p_d than the other energy transfer rates. In Figure 9
we present seasonal values of sound intensity averaged using a running
31-day boxcar filter for the 10 Hz signal. The seasonal variation shows
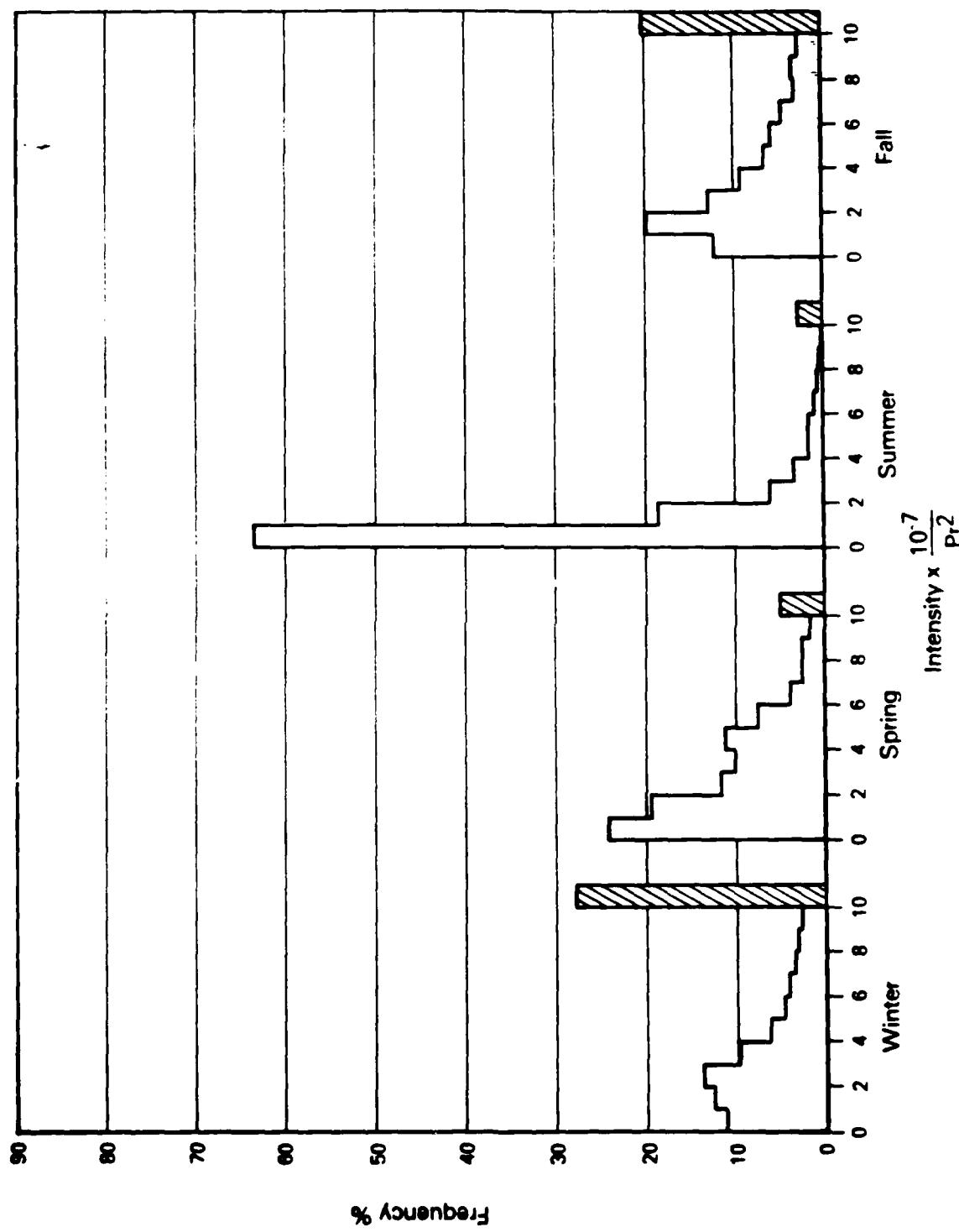
Figure 8a.   Daily Average Values of Normalized 10 Hz Sound Intensity. Vertical Scale is
Percentage of Observations During the Season at all Locations.
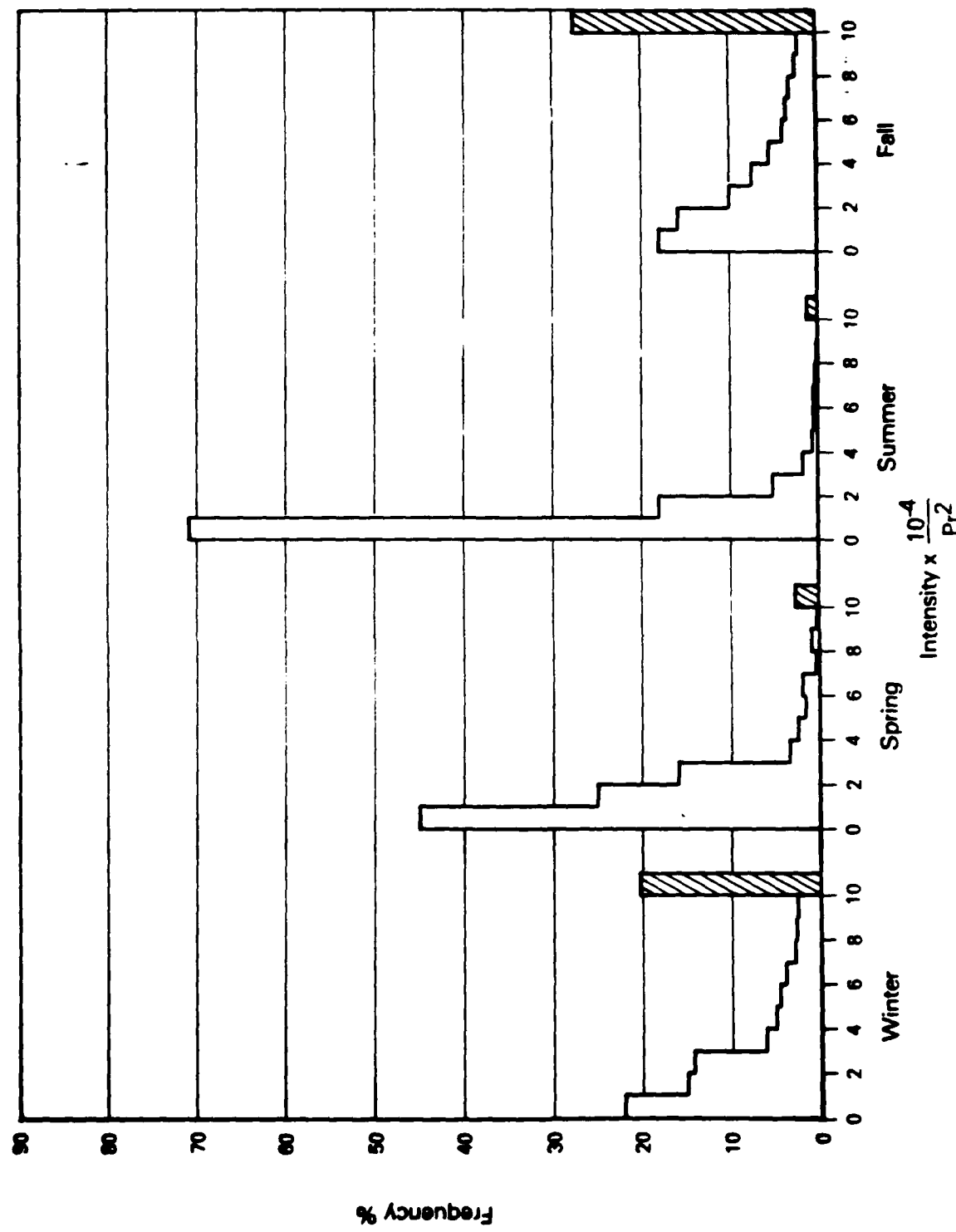
Figure 8b. Daily Average Values of 1000 Hz Sound Intensity. Vertical Scale is Percentage of Observations During the Season at all Locations.
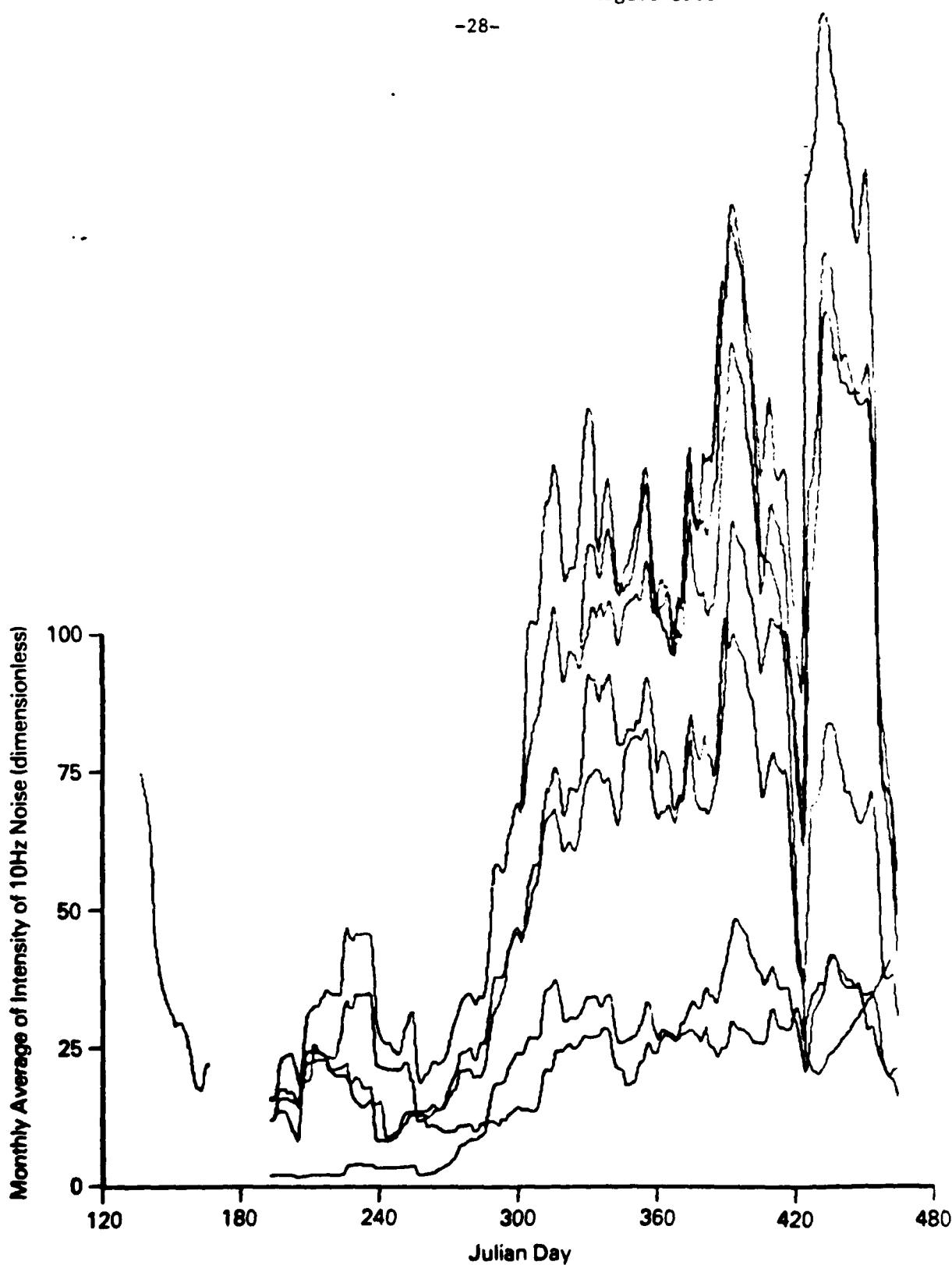
Figure 9. Time History of 31-Day Moving Average; All Stations, For 10 Hz
Normalized Sound Intensity.

up clearly. In addition, the spatial variability during winter is larger than an order of magnitude, which compares well with spatial variability of p_d . Other energy transfer rates varied much less spatially.

Although we did not take into account any transmission of sound through the ocean, it is worth noting that the two hydrophone stations nearest shore, where the largest values of p_d were computed, were two of the three largest wintertime signals in Figure 9.

During summer, strengths that are an order of magnitude or more smaller than in winter reduce the energy dissipated during deformation by a comparable factor (we observe that deformations are of the same magnitude all year). If the hypothesis that noise generation is related to the energy dissipated in ice deformation processes, then the size of this noise signal is also reduced accordingly. We, therefore, have chosen to look first at winter data and attempt to gain confidence in the energy budget when dissipation is largest.

7. Conclusions

We have looked at the atmosphere-ice-ocean energy budget in terms of average daily energy transfer at several locations over the Beaufort Sea for approximately one year. Most of the energy exchange occurs during storms lasting from 2 to 5 days. Between most storms there are usually quiet periods of similar duration.

Seasonal differences exist in all the energy exchange terms. Summer months have the largest exchange of energy from the atmosphere p_a through the ice to the ocean p_w . This is not due to increased storm activity, as can be seen in p_{afd} , but rather to decreased ice strength. For the same reason the horizontal transfer of energy p_f and the dissipation of energy by deformation p_d will be lowest during the summer free-drift period.

The maximum available energy transfer rate from the atmosphere p_{afd} is lowest during the spring and then relatively constant during summer, fall, and winter. The observed rates of energy transfer between the atmosphere and the ice p_a and between the ice and the ocean p_w are also lowest during the spring.

Spatial variability is also evident in all the observed energy transfer rates $(p_a , p_w , \text{ and } p_{afd})$. This variation is due to the horizontal dimensions of the storms relative to the observational array. Temporal offsets of storm peaks are seen between widely separated areas of the Beaufort Sea and are due to the motion of storms across the area.

Wintertime computations of the rate of energy dissipation by the ice p_d shows an even greater variation across the Beaufort Sea. Average wintertime values near the north coast of Alaska are an order of magnitude larger than those in the central or eastern Beaufort. The ability of ice to transmit energy horizontally from one location to another explains this variation.

The rate of energy dissipation cannot be computed directly from observations of motion, winds, and currents as the other energy budget terms can be. The use of an ice model to compute stresses, and all the attendant errors associated with that compuation, is necessary. This introduces some uncertainty into the computed magnitude of p_d which

was computed in this work from observed velocities at vertices of
triangles, depicting buoy stations, and a stress history by integrating
an elastic-plastic constitutive law. The spatial variability of wintertime
averages of P_d is believed to be valid and is partially confirmed by
the observed higher percentage of ridged ice near the north coast of
Alaska.

The energy content of observed acoustic signals has been examined.
Temporally, the sound energy peaks during the fall, continues high
during the winter, drops considerably during the spring, and is lowest
during the summer. This pattern corresponds to what we know and expect
of the seasonal values of energy dissipation rates in the ice cover.
Spatial variability of sound energy over the Beaufort Sea during the
winter also corresponds very closely to the variability of P_d .

The winds are one important source of energy for noise production.
Previous attempts to correlate observed noise with observed winds have
been only partially successful. The rate at which energy is transferred
from the winds to the ice appears to correlate perhaps a little better
than the winds. The introduction of horizontal energy transfer and
energy dissipation in the ice offers a reasonable explanation of the
seasonal and spatial distribution of under-ice noise.

Other energy transfers (i.e., thermal energy from the ocean and ice
to the atmosphere) have not been considered in this study. Neither did
we attempt to separate sound energy according to generating mechanisms
(i.e., thermal cracking of the ice, wind-blown snow, ocean turbulence,
or ice deformation). The results of this study are consistent with the
observation that ice deformational events (ridging, rafting, and shearing)
contribute a major portion of the energy generating background noise
in the Arctic.

References

Albright, M. (1980) "Geostrophic Wind Calculations for AIDJEX," Sea Ice
Processes and Models, R. S. Pritchard, ed., Seattle: University of
Washington Press, pp. 402-409.

—Brown, R. A. (1976) "The Resistance Law," AIDJEX Bulletin No. 31,
March.

Burke, S. P., and Buck, B. M., (1975) "The Synrams Ice Station,"
IEEE Ocean '75, pp. 413-417.

Clay, S. C., and Medwin, H. (1977) Acoustical Oceanography: Principles
and Applications, New York: John Wiley and Sons.

Coon, M. D. (1980) "A Review of AIDJEX Modeling," Sea Ice Processes
and Models, R. S. Pritchard, ed., Seattle: University of Washington
Press, pp. 12-27.

Coon, M. D., and Pritchard, R. S. (1979) "Mechanical Energy Considerations
in Sea-Ice Dynamics," Journal of Glaciology, Vol. 24, No. 90.

Coon, M. D., Maykut, G. A., Pritchard, R. S., Rothrock, D. A., and
Thorndike, A. S. (1974) "Modeling the Pack-Ice as an Elastic-
Plastic Material," AIDJEX Bulletin No. 24, May.

Greene, C. R., and Buck, B. M. (1977) "Arctic Noise Measurement Experiment
Using Nimbus 6 Data Buoys," U.S. Navy Journal of Underwater Acoustics,
Vol. 27, No. 4.

Greene, C. R., and Buck, B. M. (1978) "Influence of Atmospheric-Pressure
Gradient on Under-Ice Ambient Noise," U.S. Navy Journal of Underwater
Acoustics, Vol. 28, No. 4.

Hibler, W. D. III (1980) "Numerical Modeling of Sea Ice in the Seasonal
Sea Ice Zone," Cold Regions Science and Technology, Amsterdam:
Elsevier Scientific Publishing Company, pp. 299-321.

Leavitt, E., Albright, M., and Baumon, R. (1978) "Variations in Planetary
Boundary Layer Parameters Observed during AIDJEX," AIDJEX Bulletin
No. 39, May.

Malvern, L. E. (1969) Introduction to the Mechanics of a Continuous
Medium, Englewood Cliffs, New Jersey: Prentice-Hall.

McPhee, M. G. (1980) "An Analysis of Pack Ice Drift in Summer," Sea Ice
Processes and Models, R. S. Pritchard, ed., Seattle: University of
Washington Press, pp. 62-75.

Newton, J. L. (1973) "The Canada Basin: Mean Circulation and Intermediate-Scale Flow Features," Ph.D. dissertation, University of Washington.

Pritchard, R. S. (1975) "An Elastic-Plastic Constitutive Law for Sea Ice," Journal of Applied Mechanics, Vol. 42, No. 2, pp. 379-384.

Pritchard, R. S. (1977) "The Effect of Strength on Simulations of Sea Ice Dynamics," POAC 77, D. B. Muggeridge, ed., St. John's: Memorial University of Newfoundland, pp. 494-505.

Pritchard, R. S. (1980) "A Simulation of Nearshore Winter Ice Dynamics in the Beaufort Sea," Sea Ice Processes and Models, R. S. Pritchard, ed., Seattle: University of Washington Press, pp. 49-61.

Pritchard, R. S., Coon, M. D., and Thomas, D. R. (1979) Modeling the Mechanical Energy Budget of the Beaufort Sea Ice Cover, Flow Research Report No. 137R, Kent, Washington: Flow Research Company.

Rothrock, D. A. (1975) "The Energetics of the Plastic Deformation of Pack Ice by Ridging," Journal of Geophysical Research, Vol. 80, No. 33, November 20.

Rothrock, D. A., Colony, R., and Thorndike, A. S. (1980) "Testing Pack Ice Constitutive Laws with Stress Divergence Measurements," Sea Ice Processes and Models, R. S. Pritchard, ed., Seattle: University of Washington Press, pp. 102-113.

Thorndike, A. S., and Cheung, J. Y. (1977) "AIDJEX Measurements of Sea Ice Motion 11 April 1975 to 14 May 1976," AIDJEX Bulletin No. 35, January.

Thorndike, A. S., and Colony, R. (1977) "Estimating the Deformation of Sea Ice," POAC 77, D. B. Muggeridge, ed., St. John's: University of Newfoundland, pp. 506-517.

Thorndike, A. S., and Colony, R. (1980) "Large-Scale Ice Motion in the Beaufort Sea," Sea Ice Processes and Models, R. S. Pritchard, ed., Seattle: University of Washington Press, pp. 249-260.

Thorndike, A. S., Rothrock, D. A., Maykut, G. A., and Colony, R. (1975) "The Thickness Distribution of Sea Ice," Journal of Geophysical Research, Vol. 80, No. 33, pp. 4501-4513.

Truesdell, C. A., and Toupin, R. A. (1960) "The Classical Field Theories," Encyclopedia of Physics, Vol. III/1, S. Flügge, ed., Berlin: Springer-Verlag, pp. 226-793.

Urick, R. J. (1967) Principals of Underwater Sound for Engineers, New York: McGraw-Hill Book Company.

Wadhams, P. (1975) Sea Ice Morphology in the Beaufort Sea, Tech. Report No. 36, The Beaufort Sea Project.

Wadhams, P., and Horne, R. (1978) An Analysis of Ice Profiles Obtained
   by Submarine Sonar in the AIDJEX Area of the Beaufort Sea, Scott Polar
   Research Institute Technical Report 78-1.

Weeks, W. F., Tucker, W. B., Frank, M., and Fungcharoen, S. (1980)
   "Characterization of Surface Roughness and Floe Geometry of Sea Ice
   over the Continental Shelves of the Beaufort and Chukchi Seas,"
   Sea Ice Processes and Models, R. S. Pritchard, ed., Seattle:
   University of Washington Press, pp. 300-312.

Appendix A.   Elastic-Plastic Material Model

We introduce the AIDJEX model (Coon et al., 1974; Coon, 1980) which
describes the ice behavior by an elastic-plastic material response.
This is an approximation to rigid plastic behavior with the stiff elastic
component included more for numerical than for physical reasons.

The stress state $\underset{\sim}{\sigma}$ is required by the yield criterion

$$\phi(\underset{\sim}{\sigma}, \, p^*) \leq 0 \tag{A.1}$$

to lie within the yield surface $(\phi = 0)$. A diamond yield surface
(Figure A.1) provides accurate simulation of sea ice dynamics (Pritchard,
1977; Pritchard et al., 1979) when coupled with a normal flow rule

$$\underset{\sim}{D}_p = \lambda \, \frac{\partial \zeta}{\partial \underset{\sim}{\sigma}} \, , \tag{A.2}$$

where $\underset{\sim}{D}_p$ is plastic stretching and λ is a nonnegative scalar.
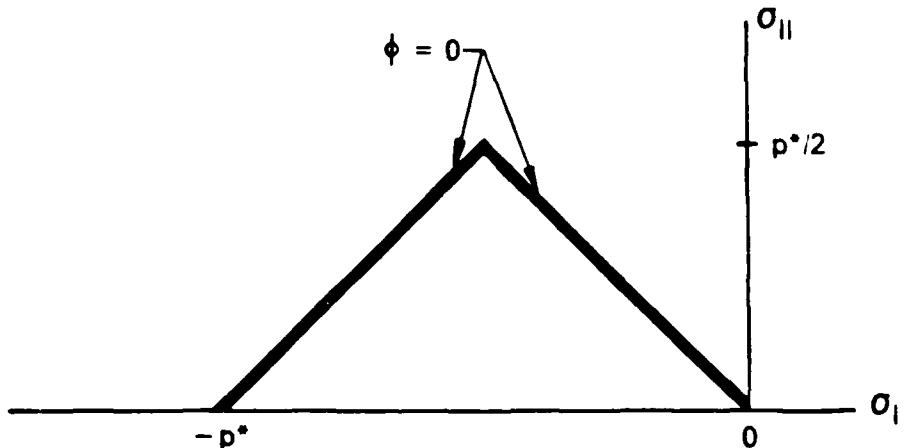
Figure A.1.   Sea Ice Yield Surface. The Axes are Stress Invariants: σ_I = 1/2 tr σ and
σ_{II} = (1/2 tr $\sigma' \sigma'$)$^{1/2}$ where $\sigma' = \sigma - \sigma_I 1$ **is the Deviatoric Stress. The
Diamond-Shaped Surface is Visualized by Rotating the Curve Around the
Abscissa, which Represents Independence of the Direction of the
Principal Stress.**

The elastic response within and on the yield curve is

$$\underset{\sim}{\sigma} = (M_1 - M_2) \underset{\sim}{1} \, \text{tr} \, \underset{\sim}{e} + 2M_2 \underset{\sim}{e} \quad , \tag{A.3}$$

where $\underset{\sim}{e}$, the elastic strain, satisfies the kinematic relationship (Pritchard, 1975)

$$\dot{\underset{\sim}{e}} - \underset{\sim}{W}\underset{\sim}{e} + \underset{\sim}{e}\underset{\sim}{W} = \underset{\sim}{D} - \underset{\sim}{D}_p \tag{A.4}$$

for stretching $\underset{\sim}{D} = \frac{1}{2}(\underset{\sim}{L} + \underset{\sim}{L}^t)$, for spin $\underset{\sim}{W} = \frac{1}{2}(\underset{\sim}{L} - \underset{\sim}{L}^t)$, and $\underset{\sim}{L} = \nabla \underset{\sim}{v}$ is the velocity gradient.

The rate of change of energy due to deformation p_d (called stress power by Truesdell and Toupin, 1960) may be decomposed for this material model by substituting Equation (A.4) into Equation (11) so that

$$p_d = \text{tr} \, \underset{\sim}{\sigma}\dot{\underset{\sim}{e}} + \text{tr} \, \underset{\sim}{\sigma}\underset{\sim}{D}_p \quad . \tag{A.5}$$

There is no contribution to p_d from spin in this formulation. The recoverable and dissipative rates of energy change are thus separated as

$$p_d = \dot{U}_e + p_\ell \quad . \tag{A.6}$$

where $\dot{U}_e$ is the rate of change of elastic strain energy

$$\dot{U}_e = \text{tr} \, \underset{\sim}{\sigma}\dot{\underset{\sim}{e}} \tag{A.7}$$

and p_ℓ is the rate of plastic dissipation by the stress during deformation

$$p_\ell = \text{tr} \, \underset{\sim}{\sigma}\underset{\sim}{D}_p \quad . \tag{A.8}$$

The elastic strain energy function U_e is a quadratic function of elastic strain (Malvern, 1969) that may be converted to stress components using Equation (A.3) giving

$$U_e = \frac{1}{2}\left(\frac{\sigma_I^2}{M_1} + \frac{\sigma_{II}^2}{M_2} \right). \tag{A.9}$$

The material constants in this work are chosen as

$$p^* = 10^5 \text{ N/m}$$
$$M_1 = 10^7 \text{ N/m}$$
$$M_2 = 0.5 \times 10^7 \text{ N/m}$$

For these values it is possible to determine an upper bound for the contribution of the rate of change of elastic strain energy to the energy budget. This contribution must be small if it is to be assumed that the elastic response is stiff enough to approximate rigid-plastic behavior. The elastic strain energy is bounded by

$$0 \le U_e \le 1/2 \frac{\left(-p^*\right)^2}{M_1} \qquad (A.10)$$

for these material constants and the diamond yield surface. If the stress state is assumed to cross the yield surface completely in a single one-day time step ($\Delta = 1$ day), then the maximum elastic strain rate is achieved. The maximum elastic strain is limited to the order of 1 percent per day by $p^*/(M_1\Delta) = 0.01$ day^{-1}. Therefore, the maximum rate of change of elastic strain energy is

$$\left|\dot{U}_e\right|_{max} = 5 \text{ mW/m}^2 \quad . \qquad (A.11)$$

DATE
FILMED

-8